Theoretical and Computational Acoustics
D. Lee, Y-H Pao, M.H. Schultz, and Y-C Teng (Editors)

Analysis of Wave Field in Fluid Entrained Between Two Concentric Cylindrical Shells

Shigeru Yoshikawa and Kenji Saijyou
5th Research Center, Technical R&D Institute, Defense Agency
3-13-1 Nagase, Yokosuka, 239 Japan

Abstract

A structure of two concentric submerged cylindrical shells whose annular space is filled with fluid is a simplified model of double-hull submersibles, and is called a *double shell.* The simply-supported boundary condition is applied to its both ends. When the inner shell is driven by a harmonic point force, the fluid-structure coupling by the annular entrained fluid yields the coupled vibration of double shell.

The following general characteristics of the standing wave field in the entrained fluid are derived from the analysis:

(1) If the evanescent radiation takes place, the phase of the K-space field pressure is expected to be constant and opposite to that of the K-space displacement of the inner driven shell. This phase relation, which seems to be characteristic of the near field, holds approximately even if the propagating radiation takes place.

(2) If the double shell vibrates in an anti-phase mode, the field pressure distribution between the inner and the outer radius shows an almost uniform pattern. This suggests a spring-like action of the field.

(3) If the double shell vibrates in an in-phase mode, the field pressure distribution shows a complicated pattern depending on the frequency and mode numbers. Particularly, a destructive interferential pattern suggests a mass-spring action of the field.

1 Introduction

The fluid-structure interaction in a point-driven *double shell* (two concentric submerged cylindrical shells coupled by the entrained fluid) was recently investigated[1, 2]. The forced vibration of the inner shell produces acoustic pressure in the entrained fluid and in turn this pressure wave drives the outer shell. A standing wave field is finally formed in the entrained fluid because of reflections at these shells. Simultaneously, the inner and outer shells can vibrate in phase or out of phase each other. These two modes of vibration yield the corresponding two separate dispersion curves.

This paper focuses on analyzing the standing wave field formed in the entrained fluid. Flügge's shell equations and Helmholtz' fluid equation are solved after the two-dimensional, spatial Fourier transform is applied to them. On the basis of this K-space transform and the modal representation, the wave field is determined after specifying the radial displacement of double shell from the boundary conditions.

2 Coupled Vibration of Double Shell

A theoretical model is shown in Fig. 1. The double shell is driven radially with a point force F_1 located at $r = R_1, \theta = 0$, and $z = z_0$ in the cylindrical coordinate system (r, θ, z). The force is harmonic and has the time dependence of $\exp(-i\omega t)$, where ω is the angular frequency and t the time. Shell thickness and mean radius are denoted by h and R, respectively. Subscript i is added to these symbols to discriminate the inner shell $(i = 1)$ from the outer shell $(i = 2)$.

Table 1 summarizes the parameter values which are used for numerical calculation. The so-called internal hysteresis loss is introduced into our theory to acount for structural energy dissipation. Also, the axial wave number k_z is converted into the discrete axial mode number m according to

$$k_z \ell = m\pi, \tag{1}$$

where the shell finiteness is introduced as shell length ℓ. This relation indicates the simply supported boundary condition at both ends.

Flügge's differential equations of the shell $(i = 1, 2)$ are transformed to algebraic 3×3 matrix equation by application of the 2-D spatial Fourier transform which transforms (θ, z) to (n, k_z), where n is the circumferential mode number. The K-space representation of fluid loading, which works as force term, is derived from the Helmholtz equation for wave propagation. The inner and outer shells are coupled through the loading by the entrained fluid. Hence, the resultant coupled vibration of double shell is formulated by 6×6 matrix equation with fluid-structure coupling elements[1, 2].

3 Wave Field in the Entrained Fluid

The fluid-structure coupling in double-shell vibration is schematically shown in Fig. 2: The forced vibration W_{1n} (K-space vibrational displacement) of the inner shell produces the pressure wave in the entrained fluid, and the effect of this wave reaches the outer shell by way of the propagator $G_{12}(r)$ and drives the outer shell; in turn this induced vibration W_{2n} of the outer shell propagates back to the inner shell by way of the propagator $G_{21}(r)$, and also contributes to the external radiation by way of $G_{22}(r)$. The wave returned to the inner shell affects its original vibration. This loop, which

determines the standing wave field, may be recognized as a kind of feedback loop in the fluid-structure interaction.

The coupling defined by the loop indicated in Fig. 2 is referred to as *strong coupling*, while the coupling defined by neglecting the returning propagator $G_{21}(r)$ as *weak coupling*[1]. The outer shell may be acoustically transparent if the coupling is weak, and acoustically opaque if the coupling is strong. Some shielding effects for radiation would be expected of the strong coupling. The experiment on a double-shell model verified the validity of strong coupling[2]. Interestingly, a theory on the external excitation in acoustic scattering of an infinite double shell suggests a transparent response of the outer shell[3]. This discrepancy between radiation and scattering responses of double shell raises a challenging future work.

If the Helmholtz equation for wave propagation is transformed to K space, we have the well-known Bessel's equation[4], which gives the following general solution of the K-space pressure:

$$P_{jn}(\xi) = a_j A_{jn}(\xi) + b_j B_{jn}(\xi), \tag{2}$$

where

$$A_{jn}(\xi) = \begin{cases} J_n(k_r r) & c > c_0, \\ I_n(k_r' r) & c \le c_0, \end{cases} \tag{3}$$

$$B_{jn}(\xi) = \begin{cases} Y_n(k_r r) & c > c_0, \\ K_n(k_r' r) & c \le c_0, \end{cases} \tag{4}$$

$$k_r = \sqrt{k_0^2 - k_z^2} = k_z\sqrt{(c/c_0)^2 - 1}, \tag{5}$$

$$k_r' = \sqrt{k_z^2 - k_0^2} = k_z\sqrt{1 - (c/c_0)^2}, \tag{6}$$

$$k_z = \omega/c, \tag{7}$$

$$k_0 = \omega/c_0, \tag{8}$$

The subscript j denotes the entrained fluid ($j = 1$) and the external fluid ($j = 2$). The variable $\xi = r\sqrt{k_0^2 - k_z^2}$, where k_0 and k_z are the acoustic wave number of fluid and the axial wave number of shell, respectively. The quantity c means the phase velocity of the helical wave propagating in the axial direction along the shell, and c_0 the sound speed in the fluid. Functions J_n and Y_n, which are the Bessel functions of the first and second kind respectively, are used in the supersonic region $c > c_0$, while I_n and K_n, which are the modified Bessel functions, are used in the subsonic region $c \le c_0$. The quantities k_r and k_r' are the radial wave number in these regions, respectively. Note that the radiation is evanescent for the subsonic region and propagating for the supersonic region.

The coefficients a_j and b_j in Eq. (2) are determined by four conditions. That is, the continuity of radial velocity at three shell-fluid interfaces and the radiation condition for the external field pressure. As the result, the K-space pressure in the entrained fluid is expressed as

$$P_{1n}(r) = G_{12}(r)W_{1n}(k_z, \omega) + G_{21}(r)W_{2n}(k_z, \omega), \tag{9}$$

where the propagators

$$G_{12}(r) = \begin{cases} \left(\frac{\omega^2\rho_0}{k_r}\right)\frac{J_n(k_r r)Y_n'(k_r R_2) - Y_n(k_r r)J_n'(k_r R_2)}{J_n'(k_r R_1)Y_n'(k_r R_2) - Y_n'(k_r R_1)J_n'(k_r R_2)} & (c > c_0), \\ \left(\frac{\omega^2\rho_0}{k_r'}\right)\frac{I_n(k_r' r)K_n'(k_r' R_2) - K_n(k_r' r)I_n'(k_r' R_2)}{I_n'(k_r' R_1)K_n'(k_r' R_2) - K_n'(k_r' R_1)I_n'(k_r' R_2)} & (c \le c_0), \end{cases} \tag{10}$$

$$G_{21}(r) = \begin{cases} (\frac{\omega^2\rho_0}{k_r}) \frac{J_n'(k_rR_1)Y_n(k_rr) - Y_n'(k_rR_1)J_n(k_rr)}{J_n'(k_rR_1)Y_n'(k_rR_2) - Y_n'(k_rR_1)J_n'(k_rR_2)} & (c > c_0). \\ (\frac{\omega^2\rho_0}{k_r'}) \frac{I_n'(k_r'R_1)K_n(k_r'r) - K_n'(k_r'R_1)I_n(k_r'r)}{I_n'(k_r'R_1)K_n'(k_r'R_2) - K_n'(k_r'R_1)I_n'(k_r'R_2)} & (c \leq c_0). \end{cases} \tag{11}$$

The phase relation between the pressure and the displacement depends on the propagators as shown in Eq. (9). First, let us assume that the radiation is evanescent ($c \leq c_0$). According to the properties of the modified Bessel functions, $G_{12}(r) < 0$ and $G_{21}(r) > 0$ always hold. Therefore, if the inner and outer shells vibrate in anti-phase, Eq. (9) gives

$$\angle P_{1n}(r) = \angle W_{1n}(k_z, \omega) - 180^\circ, \tag{12}$$

where the symbol $\angle$ denotes the phase of the quantity. That is , $\angle P_{1n}(r)$ is independent of r and opposite to $\angle W_{1n}(k_z, \omega)$. This phase relation generally holds for the near field of monopole sources or low-frequency radiator[5]. The anti-phase relation of Eq. (12) is expected even if the double shell vibrates in phase, because the field is of near field. Also, Eq. (12) approximately holds even if the radiation is propagating ($c > c_0$). These anticipations are confirmed within the scope of our numerical calculation.

4 Pressure Amplitude Distribution in the Entrained Field

The amplitude distribution of $P_{1n}(r)$ of Eq. (9) is derived from the calculation of W_{1n} and W_{2n} using the previously mentioned 6×6 matrix equation in which the driving force F_1 is supposed to be 1 N. Examples of numerical calculation on the model of Table 1 are shown in Tables 2 and 3, where W_{1n} and W_{2n} are solved by fixing the circumferential mode number n to 2 and 4, respectively, and varying the axial mode number m and the frequency. Such calculation was done for $n = 1$ to 5 and $m = 0$ to 7. Figures 3 and 4 display $20 \log |P_{1n}|$ as a function of shell radius r for $n = 2$ and 4, respectively. In each figure, the left and right frames concern the anti-phase (lower-frequency) and in-phase (higher-frequency) modes of the coupled vibration, respectively. Note that the phase change of shell vibration according to the change of m is determined by the relative position of the driving force to the shell center. Therefore, because $k_z z_0 = (1/8)m\pi$, the step decrease becomes 22.5 deg when m is increased by one. Tables 2 and 3 bear this result out except for the propagating modes.

As shown in Figs. 3(a) and 4(a), the level of the evanescent mode (cf. the column "P/E" in Tables 2 and 3) for $m \geq 1$ is below 90 dB when $F_1 = 1$ N. On the other hand, the propagating mode yields 190 dB at maximum for (0,4) mode. Since the frequency of the propagating mode is generally low, the radiation to the external field is significant in lower frequencies.

The level distribution by the anti-phase vibration is almost uniform, although Fig. 3(a) shows a nearly monotonic decrease with the increasing r, while Fig. 4(a) a monotonic increase. Such a uniform distribution suggests that the anti-phase vibration is synchronized well with an elastic or springlike action of the entrained field pressure.

Contrary to the anti-phase vibration, the in-phase vibration forms more complicated distributions as shown in Figs. 3(b) and 4(b). Particularly, there are a few modes whose pressure level tends to be null between the shells. Also, the distribution pattern strongly depends on the mode order. Moreover, the levels of the evanescent modes are generally much higher in the in-phase vibration than in the anti-phase vibration. The slope of the level change is also much steeper in the in-phase vibration than in the anti-phase vibration.

According to the previous work[2], the frequency of the in-phase double-shell vibration is quite

close to that of the forced single-shell vibration, where a single shell means a shell eliminating the outer shell from a double shell. Therefore, we are inclined to consider that the inner-shell vibration is sufficiently stronger than the outer-shell vibration [this may partly explain the decreasing steep level change in Figs.3(b) and 4(b)] and that the entrained field should show a simple pressure distribution. However, this is not the case. For example, the lowest lobar mode ($n = 2$) yields comparable vibration levels for $m = 1, 2$, and 3 as indicated in Table 2.

It should be thus improper to assume a springlike action of the entrained field in the in-phase vibration. At least we may not ignore the effect of fluid mass. A few interferential patterns of the field pressure suggests that the entrained field in the in-phase vibration may work like a mass-spring system.

5 Conclusions

A theory on the coupled vibration of a double shell as a simplified model of the submersible double-hull structure is applied to the wave-field analysis in the entrained fluid. The standing wave field is formulated on the basis of the K-space and modal representations.

For a few lower vibrational modes the wave field consists of the propagating wave which satisfies the supersonic condition; for other higher modes the field consists of the evanescent wave which satisfies the subsonic condition. The phase of the K-space pressure is constant and opposite to that of the K-space displacement of the driven inner shell, because the field is of near field.

A uniform distribution of the field pressure due to the anti-phase shell vibration suggests that the vibrations of the inner and outer shells are synchronized well with a springlike action of the field pressure. However, the in-phase shell vibration yields a few modes showing a destructive interferential pattern of the field pressure, which suggests the wave field simplified as a mass-spring system. We need more future works to explain the complicated field patterns which depend on the mode order and the relative magnitude of the in-phase shell vibration.

References

[1] S. Yoshikawa, "Fluid-structure coupling by the entrained fluid in submerged concentric double-shell vibration," J.Acoust. Soc. Jpn.(E) 14, 99-111 (1993).

[2] S.Yoshikawa, E. G. Williams, K. B. Washburn, "Vibration of two concentric submerged cylindrical shells coupled by the entrained fluid," J. Acoust. Soc. Am. 95, 3273-3285 (1994).

[3] H. Huang, "Transient responce of two fluid-coupled cylindrical elastic shells to an incident pulse," J. Appl. Mech. 46, 513-518 (1979).

[4] P.M. Morse and K.U. Ingard, *Theoretical Acoustics* (Princeton U.P., Princeton, NJ, 1968), p. 356.

[5] P.M. Morse, *Vibration and Sound* (McGraw-Hill, New York, 1948), 2nd ed., pp. 312-313.

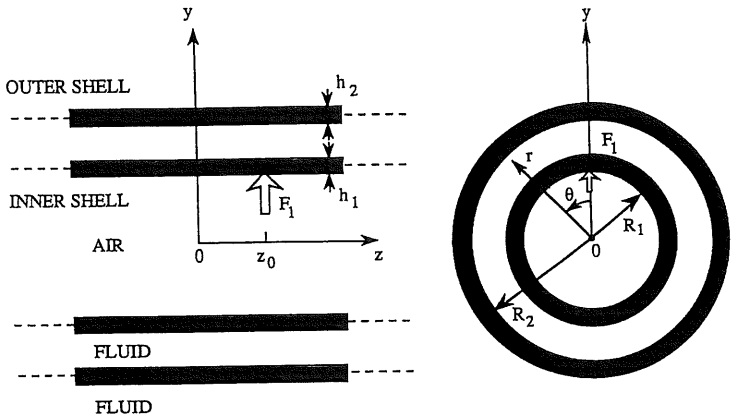

Fig. 1. Theoretical model of the double shell [2].

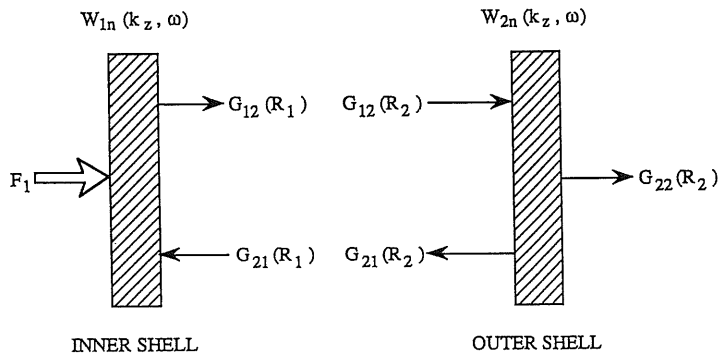

Fig. 2. Fluid-structure coupling in point-driven double-shell vibration on the basis of K-space representation [2].

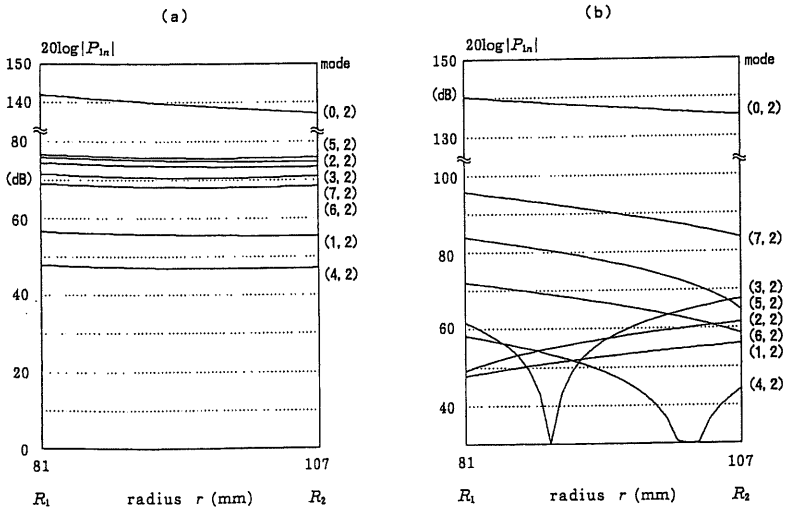

Fig. 3. Pressure distribution in the entrained fluid (n=2).
(a): anti-phase vibration; (b): in-phase vibration.

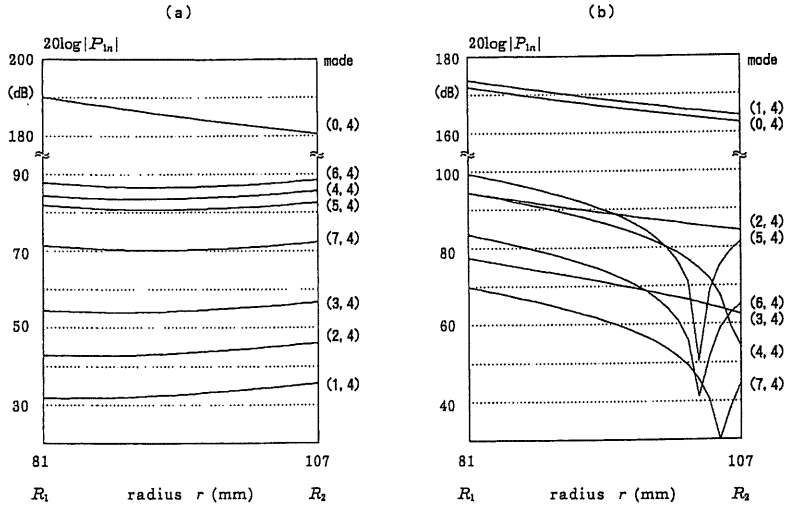

Fig. 4. Pressure distribution in the entrained fluid (n=4).
(a): anti-phase vibration; (b): in-phase vibration.

Table 1. Numerical values of double-shell model.

Inner shell		**Stainless steel**
Density	ρ (kg/m^3)	7.93×10^3
Young's modulus	E (N/m)	1.95×10^{11}
Poisson's ratio	ν	0.28
Loss factor	η	0.001
Mean radius	R_1(m)	0.081
Thickness	h_1(m)	0.003
Length	ℓ (m)	0.800
Outer shell		**Stainless steel**
Mean radius	R_2(m)	0.107
Thickness	h_2(m)	0.003
Length	ℓ (m)	0.800
Fluid		**Water**
Density	ρ_0(kg/m^3)	1.00×10^3
Sound speed	c_0(m/s)	1.4883×10^3
Driver		**Harmonic point force**
Position	z_0(m)	0.1 (from the center)

Table 2. Vibrational displacements of double shell (n = 2).

m	f (Hz)	$\lvert W_{1n} \rvert$	$\angle W_{1n}$	$\lvert W_{2n} \rvert$	$\angle W_{2n}$	P/E
0	72.10	7.91×10^{-6}	- 0.02°	4.54×10^{-5}	179.98°	P
0	200.80	1.01×10^{-2}	109.76°	4.06×10^{-3}	109.76°	P
1	204.40	4.55×10^{-3}	- 22.59°	5.68×10^{-4}	157.41°	E
1	481.40	1.61×10^{-3}	157.43°	1.72×10^{-3}	157.43°	E
2	479.10	7.59×10^{-3}	- 45.01°	1.49×10^{-3}	134.99°	E
2	964.20	9.55×10^{-4}	135.03°	9.49×10^{-4}	135.03°	E
3	896.90	1.65×10^{-3}	- 67.55°	6.97×10^{-4}	112.45°	E
3	1516.50	1.63×10^{-3}	112.61°	1.33×10^{-3}	112.61°	E
4	1342.00	3.08×10^{-5}	- 90.02°	2.30×10^{-5}	89.98°	E
4	2131.90	2.31×10^{-4}	90.06°	1.56×10^{-4}	90.06°	E
5	1768.95	4.40×10^{-4}	-112.23°	4.92×10^{-4}	67.77°	E
5	2770.35	1.97×10^{-3}	67.43°	1.15×10^{-3}	67.43°	E
6	2181.60	1.14×10^{-4}	-134.89°	1.73×10^{-4}	45.11°	E
6	3381.95	2.95×10^{-4}	45.10°	1.53×10^{-4}	45.10°	E
7	2567.95	1.07×10^{-4}	-157.46°	2.04×10^{-4}	22.54°	E
7	3956.00	2.99×10^{-3}	22.61°	1.40×10^{-3}	22.61°	E

Note 1: Column "P/E" discriminates the propagating mode (P) from the evanescent mode (E).
Note 2: The driving force F_1 = 1 Newton.

Table 3. Vibrational displacements of double shell (n = 4).

m	f (Hz)	$\lvert W_{1n} \rvert$	$\angle W_{1n}$	$\lvert W_{2n} \rvert$	$\angle W_{2n}$	P/E
0	537.10	2.60×10^{-7}	0.00°	3.07×10^{-6}	180.00°	P
0	1232.60	1.09×10^{-3}	3.12°	2.18×10^{-4}	3.12°	P
1	610.50	1.37×10^{-5}	- 22.54°	1.17×10^{-4}	157.46°	E
1	1245.30	1.91×10^{-3}	157.22°	4.04×10^{-4}	157.22°	P
2	786.65	5.11×10^{-5}	- 44.96°	2.31×10^{-4}	135.04°	E
2	1294.20	3.92×10^{-2}	135.07°	9.99×10^{-3}	135.07°	E
3	1006.85	1.94×10^{-4}	- 67.51°	4.56×10^{-4}	112.49°	E
3	1406.75	5.16×10^{-3}	112.51°	1.74×10^{-3}	112.51°	E
4	1242.40	5.38×10^{-3}	- 90.04°	7.94×10^{-3}	89.96°	E
4	1603.30	3.14×10^{-2}	89.86°	1.37×10^{-2}	90.86°	E
5	1495.65	3.18×10^{-3}	-112.55°	3.87×10^{-3}	67.45°	E
5	1870.90	4.27×10^{-2}	67.47°	2.10×10^{-2}	67.47°	E
6	1771.40	4.63×10^{-3}	-135.04°	5.83×10^{-3}	44.96°	E
6	2192.20	4.96×10^{-3}	44.95°	2.39×10^{-3}	44.95°	E
7	2063.35	5.02×10^{-4}	-157.51°	7.42×10^{-4}	22.49°	E
7	2552.15	7.28×10^{-4}	22.42°	3.16×10^{-4}	22.42°	E